Figure 1.

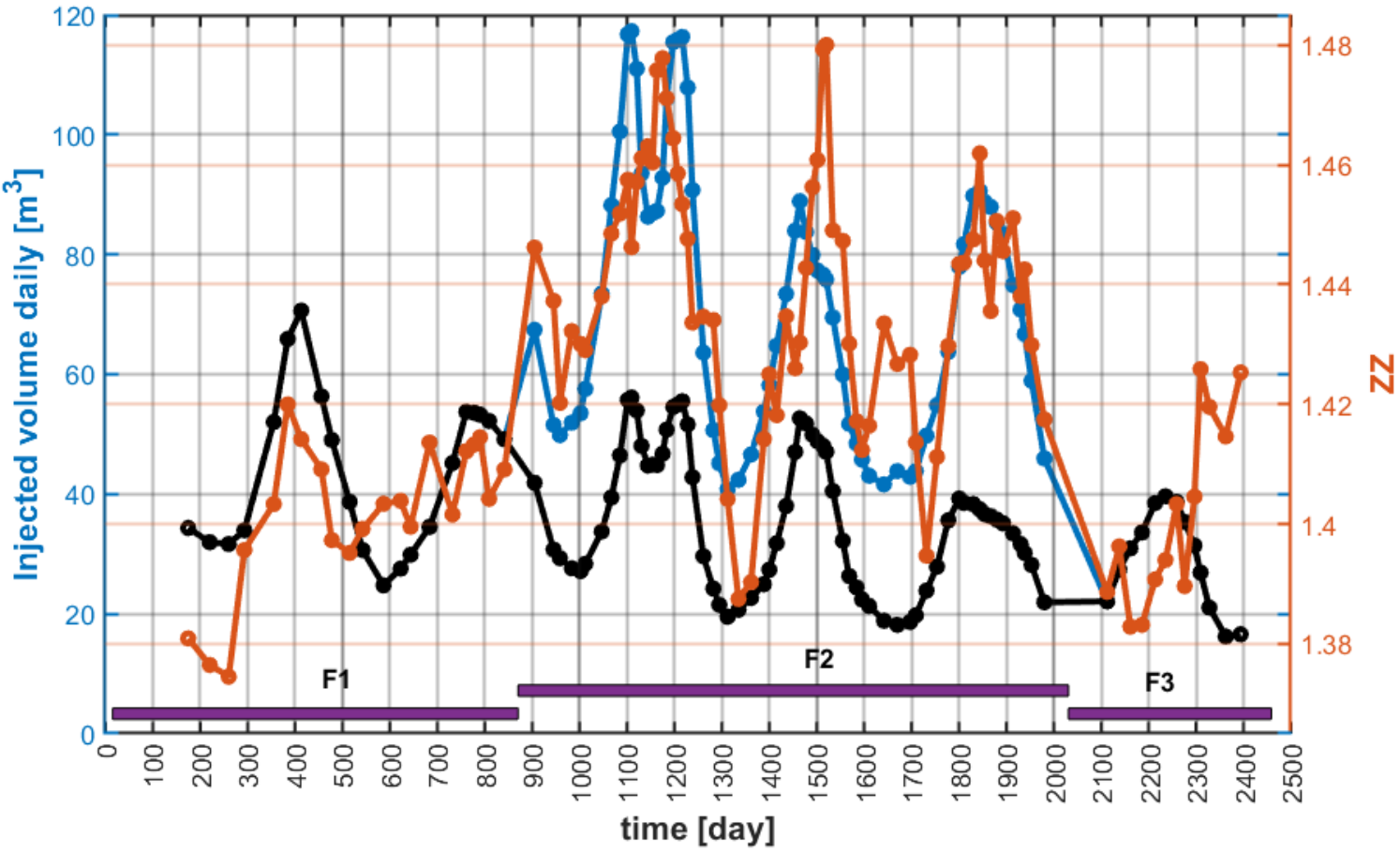
Injected volume daily [m3]
zz
time [day]
F1
F2
F3
0
20
40
60
80
100
120
1.38
1.4
1.42
1.44
1.46
1.48
0
100
200
300
400
500
600
700
800
900
1000
1100
1200
1300
1400
1500
1600
1700
1800
1900
2000
2100
2200
2300
2400
2500

Figure 2.

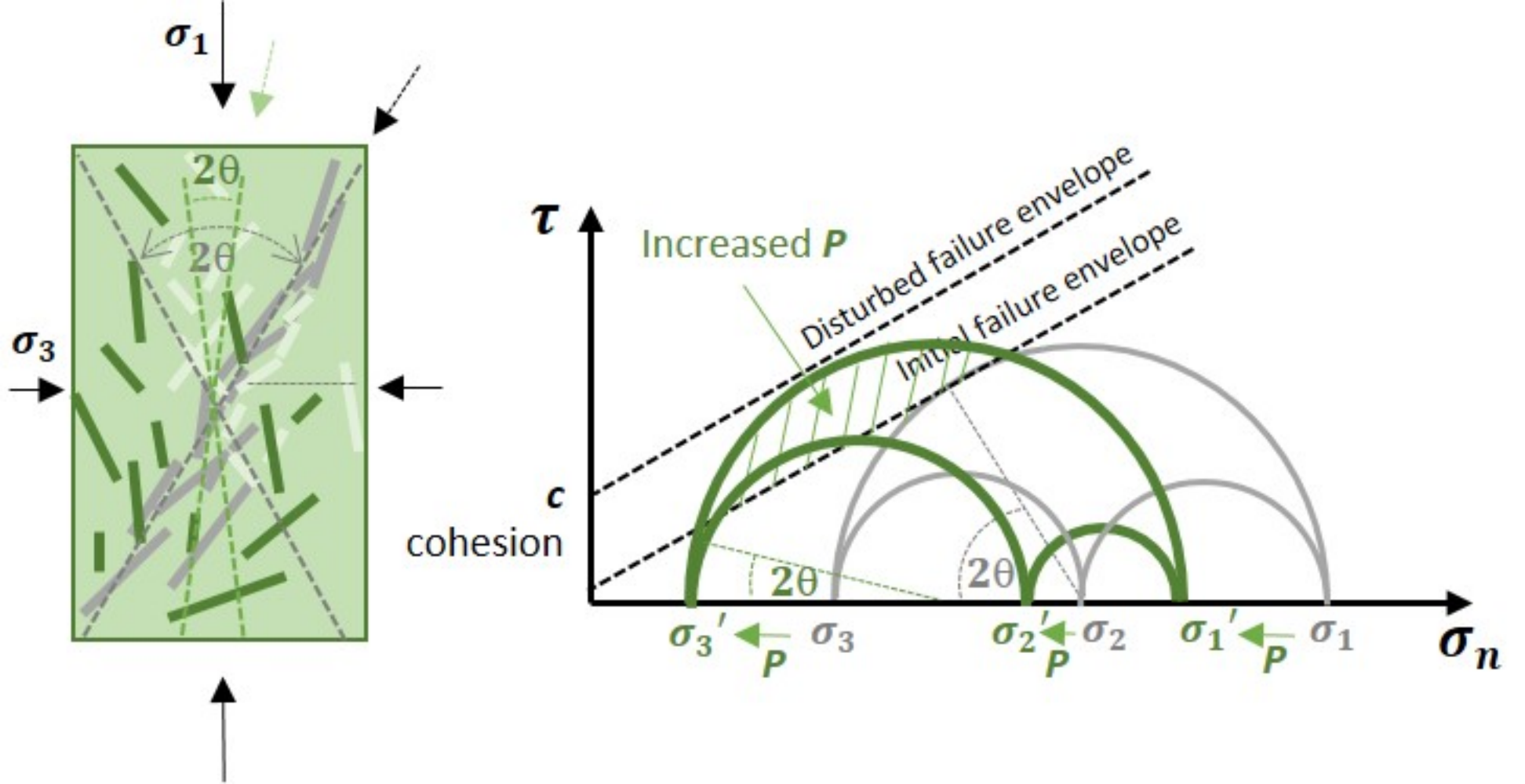
σ_1
2θ
2θ
σ_3
τ
Increased P
Disturbed failure envelope
Initial failure envelope
c
cohesion
2θ
2θ
σ_3'
P
σ_3
σ_2'
P
σ_2
σ_1'
P
σ_1
σ_n

High injection rates counteract formation of far-reaching fluid migration pathways at The Geysers geothermal field

Stanisław Lasocki [1], and Beata Orlecka-Sikora [1]

[1]Institute of Geophysics Polish Academy of Sciences.

Corresponding author: Stanisław Lasocki (lasocki@igf.edu.pl)

Key Points:

- Degree of seismic sources disorder correlates with injection rate and amplitudes of its changes agree with injection rate changes.
- Formation of long pathways for fluid migration requires certain ordering of seismic sources.
- High injection rates increase sources disorder hence decrease chance for seismic fractures to coalesce into long fluid migration pathways.

Abstract

Deep underground water injections induce seismicity. When the seismic fractures coalesce into far-reaching pathways for fluid migration, the migrating fluid may reach pre-existing faults, and by decreasing fault strength, can trigger major seismic events. We assume that the potential for building such pathways depends on closeness of hypocenters, similarity of fracture planes orientations, and closeness of radii taking off from the injection point, on which events locate. We define this potential as the average distance between seismic events in the space of parameters quantifying the above conditions. We show that in the studied case from The Geysers geothermal field, this potential is highly correlated with injection rate. When the overall level of injection rate is high, the higher the injection rate, the more the potential for building far-reaching pathways for fluid migration is reduced.

Plain Language Summary

Geothermal energy production is often based on pumping cold water down to hot rocks and taking back steam. Pressurized underground water injections induce brittle fracturing of rocks, that is seismic events, what enhances the rock permeability and in this way increases the surface on which heat exchange takes place. However, the seismic fractures may also coalesce into undesired pathways enabling the fluids to migrate far and reach pre-existing tectonically preloaded faults. Then the fluids decrease fault strength, and in result the fault can rupture producing a major seismic event. We studied how some properties of the seismicity induced by injections of water in a part of the Geysers, which can lead to the mentioned undesired fracture network development, depend on injection rates. Our studies indicated that the potential for such network development is highly correlated with the injection rate. Moreover, it turned out that in order to avoid this unwanted development of fracture network the injection rates should be kept high. The higher the injection rate is, the more the potential for building far-reaching pathways for fluid migration is reduced. These results, when confirmed on other seismically active geothermal energy production cases can have important implications for strategies of geothermics.

1 Introduction

Deep underground water injections induce seismicity. This seismic fracturing of rocks is desirable as it increases the surface on which heat exchange takes place in Enhanced Geothermal Systems. However, the seismic fractures may also coalesce into undesired pathways for fluid migration. These are such pathways that enable the fluids to reach pre-existing faults. In result, by decreasing fault strength, the fluids can trigger ruptures and produce major seismic events. The further the migration pathways extend from the injection point, the more probable are these unwanted effects. It is therefore of paramount importance to recognize under which injection conditions an induced seismic process can produce such pathways (e.g.: Davies et al., 2013; Ellsworth, 2013; Majer et al., 2012; Zhang Dongxiao & Yang Tingyun, 2015).

Numerous studies indicate that the geometry of fractures and the structure of fracture networks are the main factors controlling fluid flow and the fluid transport characteristics of rocks (e.g.: Hope et al., 2015; Lee et al., 1990; Long & Billaus, 1987; Schwartz et al., 1983; Snow, 1965). The development of the fracturing process has been investigated in a number of laboratory experiments (e.g.: Ko & Kemeny, 2011; Lockner et al., 1992; Stanchits et al., 2006). Based on these experiments, many models have been developed to simulate the geometry of

fractures and the topology of fracture networks (e.g.: Hope et al., 2015; Lee et al., 1990; Long & Billaus, 1987). However, although seismic field data provide direct insight into the development of fracture networks at the crustal scale, there are few studies focused on this topic (e.g.: Chorozoglou et al., 2018; Kagan,1992; 2000; Orlecka-Sikora et al., 2019; Sausse et al., 2010).

Here we study seismic and injection data from a part of the Geysers geothermal field to determine a relationship between the injection conditions and the potential of injection-induced seismicity to build far-reaching pathways for fluid migration. We formulate three conditions which we expect to play a role in linking fractures and building such pathways: closeness of hypocenters; similarity of fracture planes orientations; closeness of radii, which begin at the open hole section of the injection well and on which events occur. We assume that in the same injection conditions and for the same orientation of the line connecting hypocenters of two events with respect to the orientation of regional stress field, the probability for these events to link is higher when they are closer to each other than when they are farther from each other. We assume that, for the same stress and injection conditions and the same distance between hypocenters, when the fault planes of two events are parallel and they are parallel to the line connecting hypocenters, the probability for these events to link is higher than this probability for other mutual orientations of fault planes. Moreover, when they have linked they more likely extend farther than the linked fractures with other fault plane orientations. We assume that linked fractures located along the straight line beginning at the injection point reach farther from this point than such fractures located in another way.

Consequently, seismic events are represented by eight parameters: three hypocentral coordinates, three independent angles determining orientations of the T and P axes of the double-couple focal mechanisms, and two angular coordinates of hypocenters in the spherical system beginning at the open hole of injection well. To achieve the same scaling of these parameters, we transform them to equivalent dimensions (ED) (Lasocki, 2014; Supporting Information Text S1). The average distance between the events in the 8-dimensional space of the aforementioned parameters, called the degree of disordering of sources, *ZZ*, expresses to which extent the above three conditions have been fulfilled. The chance for the seismic events with small value of *ZZ*, that they link and reach far is higher than in other cases. In this way ZZ quantifies the potential for building far-reaching fluid migration pathways.

We show that *ZZ* is highly significantly correlated with injection rate. *ZZ* took the highest values when the injection rates were the highest, which indicates that high injection rates counteracted the formation of far-reaching fluid migration pathways.

2 Data and Methods

The Geysers geothermal field is located in California, US. Geothermal operations, which began there in 1960s, and which presently use EGS technology, have induced hundreds of thousands of seismic events. We studied injection and seismic data from an isolated area of 2 km × 2 km in the NW part of The Geysers, between 10 December 2007 and 23 August 2014. The basis for the seismic dataset was an improved catalog that contained 1252 events (Kwiatek et al., 2015; Martínez-Garzón et al., 2014; 2016). This catalog provided all the event parameters, necessary for the calculation of the degree of disordering of sources, *ZZ*: hypocenter locations with an accuracy of 50 m, and focal mechanisms with an accuracy of 20°/5°/10° for strike/dip/rake. The focal mechanisms were used to recover the trend and plunge angles of T and P axes. Moment magnitude was used and the completeness level was Mc=1.4 (Kwiatek et al.,

2015). The strongest event was Mw3.2. Hypocenter locations and magnitude distributions are provided in Supporting Information Figures S1-S5.

In the study period, the injections in the study area were carried out into two wells: Prati9 and Prati29. There were three phases of the injection activity:

- Phase F1 from 10 December 2007 to 10 April 2010, in which only Prati9 was operational,
- Phase F2 from 11 April 2010 to 21 June 2013 with simultaneous injections into both wells,
- Phase F3 from 11 June 2013 to the end of the study period, in which only Prati9 was operational.

The injection data consisted of the daily injection volumes into Prati9 and Prati29.

Most of the 1252 seismic events clustered around the open hole of Prati9 well (see: Supporting Information Figures S1-S4). We intended to analyze the relationship between injection and the degree of disordering of sources, *ZZ*, within the whole time period of available data, in which period only Prati9 well was constantly operational. Therefore we studied these events located closer to Prati9 well, expecting that their spatial relation to Prati9 resulted from their physical relation to the injection activity in Prati9. As the selection criterion we used the hypocentral distance from the open hole of Prati9 to be no more than 600 m. 1121 events that fulfilled this criterion are called cluster A.

The degree of disordering of sources, *ZZ*, used to quantify the potential for building the far-reaching fluid migration pathways, was the average distance between the seismic events in the 8-dimensional parameter space $\{x_1, x_2, x_3, plu\_X_1, plu\_X_2, tre\_X_1, \Theta, \varphi\}$. $x_{1,2,3}$ were hypocenter coordinates. plu_X_1, tre_X_1 were the plunge and trend angles of T axis. plu_X_2 was the plunge angle of P axis. Θ, φ were the polar and azimuthal angles of hypocenter in the spherical system of coordinates beginning at the open hole of Prati9 well. Θ=0 for the vertical direction and φ=0 for the N direction. These parameters were not comparable therefore we first transformed them to ED. The transformation to ED is a technique based on a probabilistic equivalence of the parameters that scale differently (Lasocki, 2014; Supporting Information Text S1). All transformed parameters are uniformly distributed in [0,1] and the distance between any two objects is the Euclidean metric. Further on the symbols $x_1, x_2, x_3, tre\_X_1, tre\_X_2, plu\_X_1, plu\_X_2, \Theta, \varphi$ denote the EDs of the original source parameters.

The closeness of hypocenters was parameterized by the absolute differences between hypocenter coordinates, $\Delta x_k(i,j) = |x_k(i) - x_k(j)|, k = 1,2,3.$

The trend angle and the polar angle take values in [0°, 180°], which is [0, 1] in ED, and the azimuthal angle takes values in [0°, 360°], which is also [0,1] in ED. The shortest distances between these angles in ED were therefore:

$$\Delta tre\_X_1(i,j) = 2\begin{cases} |tre\_X_1(i) - tre\_X_1(j)| & if\ \ |tre\_X_1(i) - tre\_X_1(j)| \le 0.5 \\ 1 - |tre\_X_1(i) - tre\_X_1(j)| & if\ \ |tre\_X_1(i) - tre\_X_1(j)| > 0.5 \end{cases}, \quad (1)$$

$$\Delta\theta(i,j) = 2\begin{cases} |\theta_i - \theta_j| & if\ \ |\theta_i - \theta_j| \le 0.5 \\ 1 - |\theta_i - \theta_j| & if\ \ |\theta_i - \theta_j| > 0.5 \end{cases}, \quad (2)$$

$$\Delta\varphi(i,j) = 4\begin{cases} |\varphi(i)-\varphi(j)| & if \ \ |\varphi(i)-\varphi(j)| \le 0.25 \\ \left|0.5-|\varphi(i)-\varphi(j)|\right| & if \ \ 0.25 < |\varphi(i)-\varphi(j)| \le 0.75 \\ 1-|\varphi(i)-\varphi(j)| & if \ \ |\varphi(i)-\varphi(j)| > 0.75 \end{cases}. \quad (3)$$

The multipliers in front of the opening braces in equations (1-3) were inserted so that the differences in all parameters scaled in [0, 1].

The plunge angle takes values in [0°, 90°], hence, $\Delta plu\_X_k(i,j)$ was always $|plu\_X_k(i) - plu\_X_k(j)|$, k=1,2.

For a collection of n seismic sources the degree of disordering of sources, ZZ reads:

$$ZZ = \left\{\sum_{i=1}^{n-1}\sum_{j=i+1}^{n} ZZ(i,j)\right\} / \frac{n(n-1)}{2} \quad (4)$$

where

$$ZZ(i,j) = \sqrt{[\sum_{k=1}^{3}\Delta x_k(i,j)^2] + [\Delta tre\_X_1(i,j)^2 + \sum_{k=1}^{2}\Delta plu\_X_k(i,j)^2] + [\Delta\theta(i,j)^2 + \Delta\varphi(i,j)^2]} = \sqrt{\Delta_r(i,j)^2 + \Delta_M(i,j)^2 + \Delta_\phi(i,j)^2} \quad (4a)$$

$\Delta_r(i,j)$ is the distance between hypocenters of events i and j;

$\Delta_M(i,j)$ is the distance between focal mechanisms of these two events;

$\Delta_\phi(i,j)$ is the distance between the directions of radii from the Prati9 open hole, those on which the hypocenters of these two events locate.

We carried out our analyses separately in the three injections phases. Out of 1121 studied events, 248 events occurred in the injection phase F1, 702 events – in phase F2 and 171 events – in phase F3. For every injection phase we calculated ZZ for 50-event window sliding by 10 events because the number of events per phase was not high enough to use non-overlapping windows. We obtained 21 ZZ values for F1, 66 ZZ values for F2 and 13 ZZ values for F3.

Next, we calculated the average injection rates, IN, during time windows covering the periods of the 50-event sliding windows, respectively. The calculations were performed for the injection rate periods exactly matching the periods of respective 50-event windows and for the injection rate periods from 1 to 21 days preceding the periods of event windows. The latter part of this analysis was meant to study delayed reactions of seismicity.

Finally, we studied the correlation between ZZ and IN. It comes from equation (4a) that ZZ is composed of three components representing our three conditions determining the potential of injection-induced seismicity for building far-reaching pathways for fluid migration. In order to recognize contributions of these components to the correlations between ZZ and IN we studied also the correlations between $\Delta_r, \Delta_M, \Delta_\phi$ and IN, respectively.

All correlation analyses were preceded by the Jarque-Bera test applied to check normality of the distributions of used variables. If the normality hypothesis was not rejected we used Pearson correlation, otherwise we used Spearman correlation.

We also tested differences between the values of location parameters by phase of IN, ZZ, seismic activity rate and magnitude, respectively. When the normality hypothesis for a parameter

was not rejected, we used the Student's t-test for means, otherwise we applied the Mann-Whitney U-test for medians. All statistical inferences were performed under the significance level α=0.05.

3 Results and Discussion

Some descriptive statistics by injection phase of *IN*, *ZZ*, seismic activity rate and magnitude of events are presented in Table 1 together with comparisons of their location parameters (means or medians) among phases. The medians of injection rates into Prati9 well were decreasing statistically significantly with injection phase.

Figure 1 compares the time-variations of *ZZ*, with the variations of average injection rate, *IN*. In phase F2 this comparison concerns the injection rate into Prati9 well, *IN*(9), and the total injection rate into both wells, *IN*(both). It is seen that in the first two injection phases, F1 and F2, *ZZ* correlated positively with *IN*. Also the amplitudes of the *ZZ*-changes agreed well with the amplitudes of the average injection rate changes. In phase F2, this agreement related to the summed injection into both wells (blue curve) rather than into Prati9 well alone (black curve), even though the analyzed seismic events were geometrically linked to Prati9 (Supporting Information Figures S1-S4).

Table 2 presents the results of analysis of correlations between the injection rate, *IN*, and *ZZ*. For all average injection rate series and for most *ZZ* and its components' series the normality hypothesis was not rejected. For these cases the analysis was based on Pearson's linear correlation coefficient. The exceptional cases were correlations with Δ_ϕ in phase F2 because Δ_ϕ series in this phase was not normally distributed. In these two cases Spearman's rank correlation was used.

The results in Table 2 confirm the relationships evidenced in Figure 1. In F1 and F2 the correlation between *IN* and *ZZ* was significant, positive. In F2 this correlation was highly significant, irrespective of whether the *IN* referred to injections into Prati9 or to the summed injections into Prati9 and Prati29 wells. The *ZZ* vs. *IN*(9) scatterplot is presented in Supporting Information Figure S6.

The results of correlation analysis for delayed *ZZ* with respect to *IN* are presented in Supporting Information Tables S1-S4. In F1 the correlation coefficient slowly decreases with increasing lag. The correlation coefficient in F2 slightly increased when *ZZ* was delayed with respect to *IN*, however the difference between the correlation coefficient for zero lag and for 13 days lag was only 0.022 and was surely insignificant.

The previous studies of the same data have indicated a positive correlation between seismicity rates and injection rates (Leptokaropoulos et al., 2018). Hence different time periods corresponded here to the 50-events windows; the time periods at higher injection rates were shorter. We checked whether the positive *ZZ* vs. *IN* correlations were not due to these differences between time periods. We divided phase F2 into non-overlapping windows of constant, 68 days duration. The correlation between *IN* and *ZZ* both calculated for these windows of constant time period, was also positive (0.87) and significant (p = 0.0097).

In F1 only Δ_r out of three components of *ZZ* significantly and positively correlated with *IN*. Hence, in this injection phase the positive *ZZ* - *IN* correlation resulted from that that higher injection rates were increasing distances between the sources.

In F2 all three distances, $\Delta_r, \Delta_M, \Delta_\phi$, were highly positively correlated with *IN* thus they all significantly contributed to the correlation *ZZ* – *IN*. Higher injection rates led to an increase of the distances between hypocenters, to a greater variety of P and T axes directions and to a greater angular dispersion of the hypocenters in relation to the open hole of Prati9 well.

The significant correlation Δ_r – *IN* in F1 and F2 cannot be attributed just to moving away sources from the well opening of Prati9 when the injection rates were higher. The correlation between the average distance from the Prati9 opening and *IN* was significant in F1 (corr. coefficient 0.47, p=0.03), though much weaker that the Δ_r – *IN* correlation, and in F2 it was insignificant (corr. coefficient 0.14, p=0.28).

Our target was studying the relationship between the degree of disordering of seismic sources, *ZZ*, and the injection rate, *IN*. We used the transformation to ED because the components of *ZZ*: the distances between *P* (and *T*) axes of events and the distances between radii on which events located, are not Euclidean. However, the metrics of the distance between hypocenter locations is Euclidean. Thus, it was possible to compare the shown here results of correlation between Δ_r and *IN* in F1 and F2, based on the transformation to ED, with such results based on more often used inter-event distance analyses. As alternatives to Δ_r we used correlation dimension of distances between hypocenters, D_2, and summarized squared distances in the original (*x*,*y*,*z*) space, *d2*. D_2 turned out to be uncorrelated with *IN*, probably because difficulties with its estimation. The correlation between *d2* and *IN* was even stronger than between Δ_r and *IN*. We think that this was due to the fact that any transformation, here the transformation to ED causes some loss of information. Nevertheless, the same significant correlation between *d2* and *IN* as the correlation between Δ_r and *IN* positively validated the performance of transformation to ED. The results of this part of analysis are provided and discussed in Supporting Information Text S2.

The significant impact of fluids on the stress field and the faulting regime is known from many studies (e.g., Segall and Fitzgerald,1998; Hardebeck and Hauksson, 1999; Bachmann et al., 2012). The analyses of seismic events from the NW part of The Geysers geothermal field, presented in Martínez-Garzón et al. (2013, 2016) and Kwiatek et al. (2015), clearly show a large variability of focal mechanisms. Explaining the observed stress tensor perturbation the cited authors consider the fact that in addition to fracture reactivation, massive fluid injection in EGS systems results in hydro-fracturing. It is then possible that during the time periods of higher injection rates, new small fractures were created and they could also perturb the stress field in the observed way (Martínez-Garzón et al., 2016). A number of events occurred either on severely misoriented faults (low instability coefficient, eg. Vavryčuk, 2011) or slipped in a different orientation than the predicted from the stress field. These events mostly occurred during periods of high injection rates indicating that faults not optimally oriented to the stress field require larger pore pressures to become activated.

A way in which increased injection rates may increase the degree of disordering of sources (*ZZ*) is shown schematically in Figure 2. An increase of pore pressure resulting from the increased injection rate broadens the range of possible orientations and locations for new shear fractures.

Studying fracture network development on the same data as here, Orlecka-Sikora et al. (2019) have shown that the connectivity of fractures induced by fluid injection is lower for higher injection rates and *vice versa*. Thus the connectivity was responding to the injection rate changes in the same way as *ZZ*. This allows for inferring that *ZZ* indeed represents the potential for fluid migration. In the cited work the connectivity was estimated by the connectivity coefficient, *C*, defined by the ratio of the observed number of intersections of fractures in a fracture network to the number of all possible intersections in this network. These all possible intersections were evaluated as $0.5f(f-1)$, where *f* was the number of fractures building the fracture network (Albert & Barabasi, 2002; Watts & Strogatz, 1998).

Prati29 well was operational only in phase F2. In this phase the amplitudes of *ZZ* changes agreed with the amplitudes of changes of the summarized injections into Prati9 and Prati29. Furthermore, the mean level of *ZZ* and the mean seismic activity were the highest in this phase and significantly higher than in phases F1 and F3. In F2 only the level of total injection into Prati9 and Prati29 was the highest, and the mean level of injection rate into the Prati9 well was significantly smaller than in phase F1. All these indicate the important role of the injections into Prati29 for the generation of seismic events within the studied cluster A despite the Prati29 well location being outside cluster A.

The seismic events generated at higher injection rates, i.e. the ones more disordered (*ZZ* was higher), did not have greater magnitudes. On the contrary, in phase F1 the mean magnitude in windows correlated negatively with *ZZ* (corr. coef. -0.61, $p = 0.003$). In F2 no magnitude – *ZZ* correlation was ascertained.

In phase F3, in which the overall level of injection rate was the lowest among injection phases, the correlation *IN* - *ZZ*, was significant, negative. This correlation was achieved only jointly by the three components of *ZZ*: $\Delta_r, \Delta_M, \Delta_\phi$ because neither of them significantly correlated with *IN*. The negative correlation coefficient in F3 increased when *ZZ* was delayed with respect to *IN*, and for 4 and more days lag it became statistically not significant (Supporting Information Table S4). This reversal of correlation results may be connected with another fracture mechanism below a certain level of injection rate. We discuss this possibility in Supporting Information Text S3. However, the data series in F3 was composed of only 13 points therefore the correlation ($p \approx 0.03$) might be spurious.

4 Conclusions

Studying the actual field data we found exceptionally high and immediate correlation between the injection rate and the seismicity parameter - the degree of disordering of sources, *ZZ*. Also the amplitudes of *ZZ*-changes agreed well with the amplitudes of average injection rate changes. *ZZ* is defined solely on parameters of seismic sources. It describes how much seismic fractures are dispersed in terms of distances between their hypocenters, mutual orientations of their fracture planes, and angular dispersion of their hypocenters. In the next work we will modify *ZZ* to account also for source sizes.

We interpret *ZZ* as a measure of the potential of seismic fractures for building far-reaching pathways for fluid migration. The logic of the three conditions, on which *ZZ* is based, supports this interpretation. However, ZZ does not represent all possibilities for building such a fracture system neither it is adequate for other possibilities of fracture network development (e.g. not for a percolating fluid pathway).

In the studied case from The Geysers geothermal field, the optimal conditions to avoid such ordering of seismic fractures that enable linking them into longer pathways, extending farther from the injection point were met for high injection rates. The higher the injection rate was, the more disordered the seismic fractures were generated, i.e., the chances to build longer pathways for undesired fluid migration decreased. High injection rates caused an increase in seismic activity, nevertheless the median level of seismic event magnitudes remained unaffected.

The above conclusion, if confirmed in other cases of injection induced seismicity, would help to understand this type of seismicity and related hazards. Martínez-Garzón, et al. (2018) conclude that the used here dataset from the NW region of The Geysers well represents the broader seismic processes at The Geysers field. Thus our results may be also valid for all seismic processes at The Geysers. However, for further generalizations studies of other injection-induced seismicity cases are required.

Acknowledgments

We thank the Calpine Corporation for providing high-resolution hydraulic data from The Geysers field. The comments and suggestions of two anonymous Reviewers were much appreciated. This work was supported under the S4CE: "Science for Clear Energy" project, which has received funding from the European Union's Horizon 2020 research and innovation programme, under grant agreement No 764810. The work was also partially supported by statutory activities No 3841/E-41/S/2018 of the Ministry of Science and Higher Education of Poland. Data are available on the IS-EPOS platform of Thematic Core Service Anthropogenic Hazards (https://tcs.ah-epos.eu/#episode:THE_GEYSERS_Prati_9_and_Prati_29_cluster, doi: 10.25171/InstGeoph_PAS_ISEPOS-2017-011).

References:

Albert, R. & Barabasi, A.L. (2002) Statistical mechanics of complex network, *Reviews of Modern Physics*, 74, 47–97.

Bachmann, C.E., Wiemer, S., Goertz-Allmann, B.P. & Woessner, J. (2012) Influence of pore-pressure on the event-size distribution of induced earthquakes, *Geophysical Research Letters*, 39, L09302, doi:10.1029/2012GL051480

Chorozoglou, D., Kugiumtzis, D., & Papadimitriou, E. (2018) Testing the structure of earthquake networks from multivariate time series of successive main shocks in Greece, *Physica A*, 499, 28–39.

Davies, R., Foulger, G., Bindley, A., & Styles, P. (2013) Induced seismicity and hydraulic fracturing for the recovery of hydrocarbons, *Marine and Petroleum Geology*, 45, 171-185.

Ellsworth, W.L. (2013) Injection-induced earthquakes, *Science*, 341, 6142, doi: 10.1126/science.1225942

Hardebeck, J.L. & Hauksson, E. (1999) Role of fluids in faulting inferred from stress field signatures. *Science* 285 (5425), 236-239, DOI: 10.1126/science.285.5425.236

Hope, S.M., Davy, P., Maillot, J., Le Goc, R., & Hansen, A. (2015) Topological impact of constrained fracture growth. *Frontiers in Physics* 3-75.

Kagan, Y.Y. (1992) Correlations of earthquake focal mechanisms. *Geophysical Journal International*, 110, 305-320.

Kagan, Y.Y. (2000) Temporal correlations of earthquake focal mechanisms. *Geophysical Journal International*, 143, 881-897.

Ko, T.Y., & Kemeny, J. (2011) Subcritical crack growth in rocks under shear loading. *Journal of Geophysical Research, Solid Earth*, 116, B01407, doi:10.1029/2010JB0008461.

Kwiatek, G., Martínez-Garzón, P., Dresen, G., Bohnhoff, M., Sone, H., & Hartline, C. (2015) Effects of long-term fluid injection on induced seismicity parameters and maximum magnitude in northwestern part of The Geysers geothermal field. *Journal of Geophysical Research, Solid Earth*, 120, 7085–7101, doi: 10.1002/2015JB012362.

Lasocki, S. (2014) Transformation to equivalent dimensions – a new methodology to study earthquake clustering. *Geophysical Journal International*, 197 (2), 1224-1235.

Lee, J.S., Veneziano, D., & Einstein, H.H. (1990) "Hierarchical fracture trace model" In Rock Mechanics Contributions and Challenges: Proceedings of the 31st US Symposium on Rock Mechanics, W. Hustrulid, W., & Johnson, G.A., Eds. (A.A. Balkema 1990), pp. 261-268.

Leptokaropoulos, K., Staszek, M., Lasocki, S., Martínez-Garzón, P., & Kwiatek, G. (2018) Evolution of seismicity in relation to fluid injection in the North-Western part of The Geysers geothermal field. *Geophysical Journal International*, 212, 1157–1166, doi: 10.1093/gji/ggx481

Lockner, D.A., Byerlee, J., Kuksenko, V., Ponomarev, A., & Sidorin, A. (1992) "Observations of quasi-static fault growth and acoustic emissions" in Fault Mechanics and Transport Properties of Rocks, B. Evans and T.-F. Wong, Eds. (Academic, London 1992), pp. 3–31.

Long, J.C.S., & Billaus, D.M. (1987) From field data to fracture network modeling: An example incorporating special structure, *Water Resources Research*, 23(7), 1201-1216.

Majer, E., Nelson, J., Robertson-Tait, A., Savy, J., & Wong, I. (2012) Protocol for Addressing Induced Seismicity Associated with Enhanced Geothermal Systems, *Geothermal Technologies Program U.S. Department of Energy, Energy Efficiency & Renewable Energy*

Martínez-Garzón, P., Bohnhoff, M., Kwiatek, G. & Dresen, G. (2013) Stress tensor changes related to fluid injection at The Geysers geothermal field, California, *Geophysical Research Letters*, 40, 2596–2601, doi:10.1002/grl.50438

Martínez-Garzón, P., Kwiatek, G., Sone, H., Bohnhoff, M., Dresen, G., & Hartline, C. (2014) Spatiotemporal changes, faulting regimes, and source parameters of induced seismicity: A case study from The Geysers geothermal field. *Journal of Geophysical Research. Solid Earth*, 119, 8378–8396, doi: 10.1002/2014JB011385.

Martínez-Garzón, P., Kwiatek, G., Bohnhoff, M., & Dresen, G. (2016) Impact of fluid injection on fracture reactivation at The Geysers geothermal field, *Journal of Geophysical Research. Solid Earth*, 121(10), 7432–7449, doi: 10.1002/2016JB013137.

Martínez-Garzón, P., Zaliapin, I., Ben-Zion, Y., Kwiatek, G. & Bohnhoff, M. (2018) Comparative study of earthquake clustering in relation to hydraulic activities at geothermal fields in California. *Journal of Geophysical Research. Solid Earth*, 123, 4041–4062, https://doi.org/10.1029/2017JB014972.

Orlecka-Sikora, B., Cielesta, S., & Lasocki, S. (2019) Tracking the development of seismic fracture network from The Geysers geothermal field. *Acta Geophysica*, 67, 341-350.

Sausse, J.C., Dezayes, C., Dorbath, L. Genter, A., & Place, J. (2010) 3D model of fracture zones at Soultz-sous-Forêts based on geological data, image logs, induced microseismicity and vertical seismic profiles. *Comptes Rendus Geo-sciences*, 342(7-8), 531-545.

Schwartz, F.W., Smith, L. & Crowe, A.S. (1983) A stochastic analysis of macroscopic dispersion in fractured media, *Water Resources Research*, 19(5), 1253-1265.

Segall, P. & Fitzgerald, S.D. (1998) A note on induced stress changes in hydrocarbon and geothermal reservoirs. *Tectonophysics*, 289, 117–128.

Snow, D.T. (1965) A parallel plate model fractured permeable media, PhD. Thesis, Univ. of Calif., Berkeley.

Stanchits, S., Dresen, G., & Guéguen, Y. (2006) Ultrasonic velocities, acoustic emission characteristics and crack damage of basalt and granite, *Pure Applied Geophysics*, 163(5–6), 975–994.

Vavryčuk, V. (2011) Principal earthquakes: theory and observations from the 2008 West Bohemia swarm, *Earth and Planetary Science Letters*, 305, 290–296, doi: 10.1016/j.epsl.2011.03.002.

Warren-Smith, E., Fry, B., Wallace, L., Chon, E., Henrys, S., Sheehan, A., Mochizuki, K., Schwartz, S., Webb, S. & Lebedev, S. (2019) Episodic stress and fluid pressure cycling in subducting oceanic crust during slow slip. *Nature Geoscience*, 12, 475–481, doi.org/10.1038/s41561-019-0367-x.

Watts, D.J. & Strogatz, S.H. (1998) Collective dynamics od “small-world” networks, *Nature*, 393, 440–442.

Zhang Dongxiao & Yang Tingyun (2015) Environmental impacts of hydraulic fracturing in shale gas development in the United States, *Petroleum Exploration and Development*, 42(6), 876–883.

Tables:

Table 1. Descriptive statistics and comparisons of the average injection rate, *IN*, the degree of disordering of seismic sources, ZZ, the activity rate, and magnitude of events in the three injection phases. The magnitude was transformed to the equivalent dimension. The other quantities: *IN* and activity rate were not. The column "Comparisons" contains *p*-values of the tests of differences between means or medians of these parameters. The significant differences are in bold.

	Injection phase									**Comparisons of location parameters, *p*-value**		
	F1			**F2**			**F3**			**F1 vs. F2**	**F2 vs. F3**	**F1 vs. F3**
	Mean	**Med.**	**Std. dev.**	**Mean**	**Med.**	**Std. dev.**	**Mean**	**Med.**	**Std. dev.**			
Prati9 *IN* [100m^3/day]	43.76	45.18	13.09	36.18	35.69	11.51	29.10	30.95	8.18	**0.024**	**0.014**	**3E-4**
Summed Prati9 and Prati29 *IN* [100m^3/day]	43.76	45.18	13.09	72.82	73.43	22.54	29.10	30.95	8.18	----------		
ZZ	1.402	1.403	0.012	1.439	1.438	0.021	1.401	1.396	0.015	**5E-14**	**2E-7**	0.91
Activity rate [event/day]	0.35	0.34	0.13	0.70	0.69	0.23	0.48	0.44	0.11	**7E-12**	**6E-6**	**7E-3**
Magnitude	0.55	0.57	0.06	0.49	0.49	0.04	0.45	0.47	0.06	**3E-4**	0.055	**2E-4**

Table 2. Results of the correlation analysis between the average injection rate, *IN*, and *ZZ*, and its components, $\Delta_r, \Delta_M, \Delta_\phi$. For phase F2 row 'a' provides the correlation between *ZZ* and *IN* into Prati9 well, and row 'b' provides the correlation between *ZZ* and total *IN* into Prati9 and Prati29 wells. The significant correlations are in bold. The results based on Spearman rank correlation are in italics.

Injection phase	***ZZ***		Δ_r		Δ_M		Δ_ϕ	
	Corr. coef.	***p*-value**	**Corr. coef.**	***p*-value**	**Corr. coef.**	***p*-value**	**Corr. coef.**	***p*-value**
F1	**0.62**	**0.002**	**0.69**	**$5\cdot10^{-4}$**	0.20	0.37	-0.28	0.22
F2 – a	**0.76**	**$2\cdot10^{-13}$**	**0.69**	**$2\cdot10^{-10}$**	**0.41**	**$7\cdot10^{-4}$**	***0.49***	***$3\cdot10^{-5}$***
F2 – b	**0.72**	**$7\cdot10^{-12}$**	**0.65**	**$1\cdot10^{-9}$**	**0.45**	**$1\cdot10^{-4}$**	***0.47***	***$8\cdot10^{-5}$***
F3	**-0.60**	**0.029**	-0.20	0.51	-0.32	0.28	-0.19	0.52

Figure captions:

Figure 1. Comparison of the time-variation of *ZZ* with the time-changes of average injection rate. Black – the injection rate into Prati9 well, blue – the total injection rate into Prati9 and Prati29 wells, brown – *ZZ*. The horizontal bars mark the durations of injection phases.

Figure 2. Schematic presentation of influence of pore pressure (P) changes on the failure plane orientations. The linear failure criterion imposes that shear fractures make with σ_1 a well-defined angle of (±) 45°−φ/2, where φ is the angle of internal friction, and θ=ϕ/2+45 (gray circle in Coulomb-Mohr diagram and gray fractures on the rock block on the left). An increase of P reduces the effective normal stress, σ_n', where $\sigma_n' = \sigma_n - P$ and broadens the range of possible orientations for new shear fractures (all directions going through green hatched area in the Coulomb-Mohr diagram and green fractures on the rock block) (after Warren-Smith et al., 2019).